

EMITTANCE MEASUREMENT AND MODELING FOR THE FERMILAB BOOSTER

X. Huang* and S.Y. Lee, Indiana University, Bloomington, IN 47405, USA,
K.Y. Ng, Fermilab, Box 500, Batavia, IL 60510, USA

Abstract

We systematically measured the emittance evolution of a fast cycling proton accelerator on a turn-by-turn basis under various beam intensities via an ionization profile monitor (IPM). The vertical emittance growth rate was derived and phenomenologically analyzed. The transverse and longitudinal components in the horizontal beam size were separated by making use of their different evolution behaviors. The quadrupole mode beam size oscillation after transition crossing is also studied and explained. We found a considerable space-charge-induced emittance growth rate component in the vertical plane but not as much for the horizontal plane. We carried out multiparticle simulations to understand the mechanism of space-charge-induced emittance growth. The major sources of emittance growth were found to be the random skew-quadrupole and dipole field errors in the presence of large space-charge tune spread.

INTRODUCTION

Emittance growth for beams under space charge effect is an important subject of beam physics. The increased emittance would directly affect the performance of the accelerators and potentially lead to beam loss. Proton beam loss at high energy poses a radiation safety issue. For the Fermilab Booster, a fast-cycling synchrotron, beam loss has been a limiting factor for the maximum proton production.

There are many simulation codes that address the space charge effect. But systematic emittance growth measurements are relatively few, especially for fast ramping circular accelerators. In this study, we carried out turn-by-turn emittance measurement for the Fermilab Booster with beam intensity varying from low to high to study the space charge effect. The relevant machine parameters were recorded to build a realistic machine model for the entire cycle for analysis. Emittance growth rate was derived. The vertical emittance growth rate was found to be correlated with the space-charge perveance defined as $K_{sc} = 2Nr_0/(\beta^2\gamma^3)$, where N is the number of particles per bunch, r_0 the classical proton radius and β, γ are Lorentz factors. The longitudinal component in horizontal beam size before and after transition crossing was also identified and analyzed.

We also performed simulation in attempt to understand the mechanism of space charge-induced emittance growth. The existing space-charge simulation codes are usually based on particle-in-cell (PIC) models. The need to solve the Poisson equation for space charge field makes them necessarily slow when being used to simulate thousands of

turns with $\geq 10^5$ particles. It is very difficult to vary parameters in a wide range to observe a trend or find a correlation. Therefore in our study we employ a simple model of space charge field which uses the space charge potential of a Gaussian beam. Even though this is not a self-consistent approach since the beam deviates from the Gaussian distribution due to space charge effects, we believe this method still gives useful insights to the underlying mechanism because the deviation becomes large only when an unfavorable resonance condition is met. A more detailed account of this study can be found in Ref. [1].

EXPERIMENTAL OBSERVATIONS

The Fermilab Booster is a fast ramping proton synchrotron which ramps from 400 MeV to 8 GeV in 1/30 s. It typically delivers 4×10^{12} protons per pulse. The circumference is 474.2 m with a 24-fold periodicity. The rf harmonic number is 84. The nominal tunes are 6.7 (horizontal) and 6.8 (vertical), respectively. There are 20,000 turns total in a cycle. The beam crosses transition at about the 9600th turn when $\gamma = 5.48$.

The Booster is equipped with two ionization profile monitors (IPM), one for each transverse plane. Both IPMs are located in the same region at which $\beta_x = 6.5$ m, $\beta_z = 20.5$ m and the horizontal dispersion $D_x = 1.8$ m. The transverse profile data were fit to a Gaussian plus polynomial model to extract the rms beam size [2]. The calibration routine with linear parameterization was used to compensate the space charge-induced systematic error on beam widths [2]. Such error is more severe for the horizontal plane since the horizontal beam size is smaller at the IPM location. The residual error after correction is also larger for the horizontal plane.

The Booster adopts a multi-turn H^- injection scheme. The number of injection turns indicates the initial charge that go into the Booster. Typically 10 or 11-turn injection are used for normal operation. In the experiment we intentionally changed the number of injection turns from 2 to 18, with initial charge ranging from 1.0×10^{12} to 8×10^{12} protons. However, for 15-turn injection and above, the initial charge got lost quickly in the first few hundreds of turns. The intensity signals for odd number injection turns are plotted in Fig. 1. The vertical rms emittance is derived from the beam size with $\epsilon_{z,rms} = \frac{\sigma_z^2}{\beta_z}$. As beam energy ramps up, emittance is damped down adiabatically. However, the normalized emittance $\epsilon_n = \beta\gamma\epsilon$ usually grows due to nonconservative mechanisms. Fig. 2 shows the evolution of the vertical rms emittance and normalized rms emittance in the full cycle for a weak intensity case (4-turn) and a high intensity case (12-turn). Excluding the

* xiahuang@slac.stanford.edu, Now at SLAC, Menlo Park, CA 94025

region close to extraction, we found the emittance growth behaves differently in the space charge-dominated region (region A, from beginning to turn 4000) and later in the cycle (region B, from turn 4001 to 17000) when space charge effect is less important due to the increased beam energy. In region B the growth is linear with time. We have fitted the emittance growth to a linear model and obtained the growth rate defined as $\Delta\epsilon_n/\Delta N$ for all data sets. The result is plotted in Fig. 3. The growth rate is correlated with the total charge in this region. For 10-turn injection the growth rate is 1.2×10^{-4} mm-mrad/turn before transition and 2.0×10^{-4} mm-mrad/turn afterwards. Such a large linear growth rate cannot be explained by residual gas scattering or intrabeam scattering. It is still a mystery for us.

Vertical emittance growth in region A is shown in Fig. 4. For 14-turn injection and up we observed rapid emittance blowup in the first few hundreds turns, accompanied by considerable beam loss. However, for 12-turn injection and below, the behavior is quite regular. We fit the growth with a phenomenological model by assuming the instantaneous growth rate is proportional to the space-charge perveance K_{sc} , i.e., $\frac{d\epsilon}{dt} = b_1 + b_2 K_{sc}$, or

$$\epsilon_z = a_0 + b_1 t + b_2 \int_0^t K_{sc} dt', \quad (1)$$

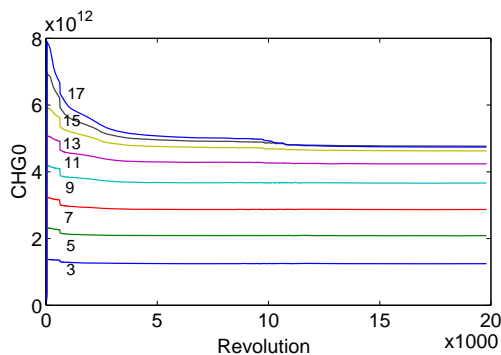


Figure 1: The total charge in a full cycle for odd number injection turns.

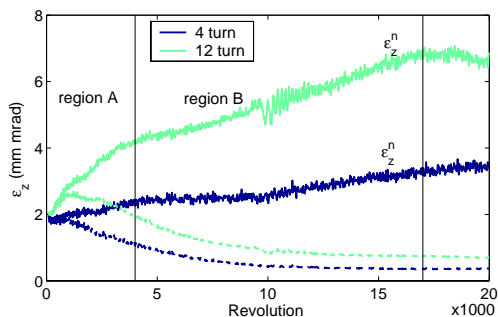


Figure 2: The vertical rms emittance (dashed) and normalized rms emittance (solid) for 4-turn and 12-turn injection.

where t is the turn number, a_0 represents the initial normalized emittance, b_1 and b_2 represent the linear and space-charge-induced growth, respectively. This model fits data with 2-turn up to 11-turn injection very well. Fig. 5 shows a typical fitting curve. The fitting results are shown in Fig. 6. The fitted initial normalized emittance ranges from 1.6 to 2.0π mm mrad. The linear growth rate agrees well with those found in region B before transition (see Fig. 3). The space-charge-induced growth rate is nearly constant because the intensity is absorbed by the perveance parameter.

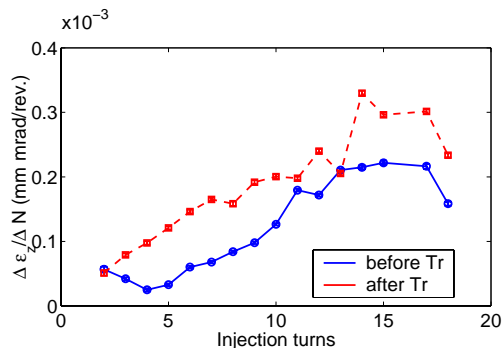


Figure 3: The linear growth rate for vertical normalized rms emittance in region B.

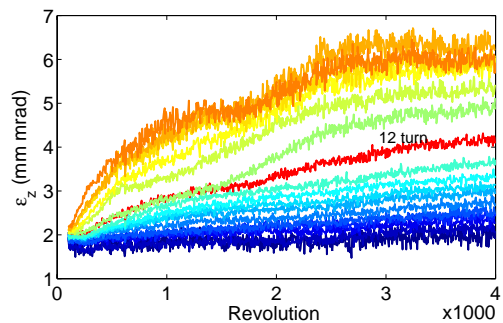


Figure 4: The normalized vertical emittance from the 70th turn to the 4000th turn for 2-turn to 18-turn injection.

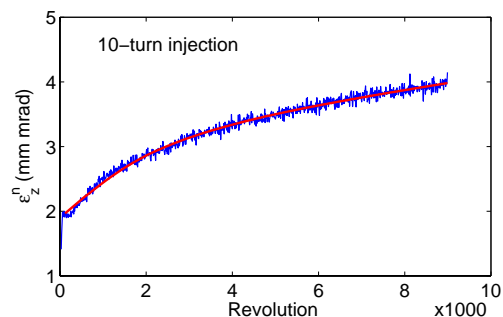


Figure 5: A typical fitting curve for vertical normalized emittance growth with Eq. (1).

The horizontal beam size consists of two components, the horizontal emittance and the momentum spread,

$$\sigma_x^2 = \beta_x \epsilon_{x,\text{rms}} + D^2 \sigma_\delta^2. \quad (2)$$

Typical horizontal beam size data in the full cycle are shown in Fig. 7. No big difference in beam size for the low and high intensity cases is seen in the space charge-dominated region. Since the momentum spread varies on the ramp according to the changing beam energy and rf gap voltage and the longitudinal emittance was not measured initially, the horizontal emittance cannot be readily derived from the measured beam size. However, noting that the two terms in Eq. (2) scale with time (hence energy, phase slip factor, rf gap voltage, etc) differently, we successfully separated them by a fitting approach. We fit the data from turn 3001 to turn 9200 to avoid the initial few ms and the region close to transition crossing. The fitting model worked well for moderate intensities (10-turn injection and below) but not for higher intensities because of larger IPM calibration errors (see Ref. [[2]]). The horizontal normalized rms emittance (Fig. 8) was found to be around 2π mm mrad at turn 3001. The growth rate ranged between 0.5×10^{-4} to 0.8×10^{-4} . The momentum spread at turn 3001 was

nearly 1.0×10^{-3} for all data set. Assuming a longitudinal 95% phase space area of 0.08 eV-s, the momentum spread is predicted to be 1.4×10^{-3} according to the ramping energy and rf curves. We have also measured the bunch length with the resistive wall monitor signal and a high-resolution oscilloscope from which we derived the momentum spread to be 1.25×10^{-3} at turn 3001.

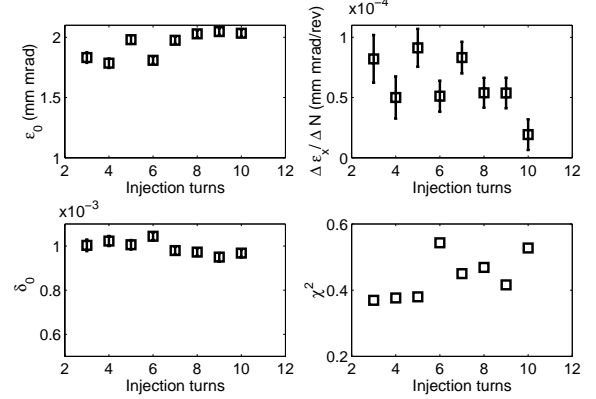


Figure 8: The normalized horizontal rms emittance at turn 3001, emittance growth rate, the momentum spread at 3001 as fitted and the residual χ^2 .

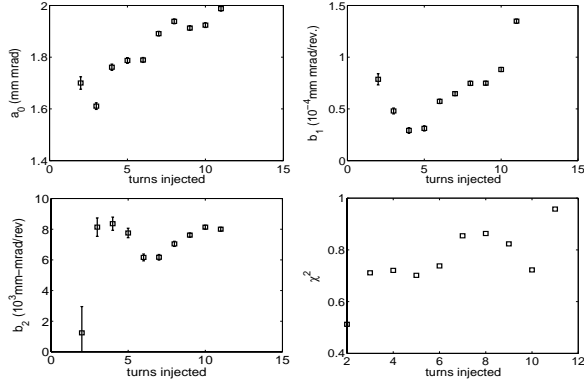


Figure 6: The fitted parameters as defined in Eq. (1) and the residual χ^2 normalized by noise sigma and number of data points.

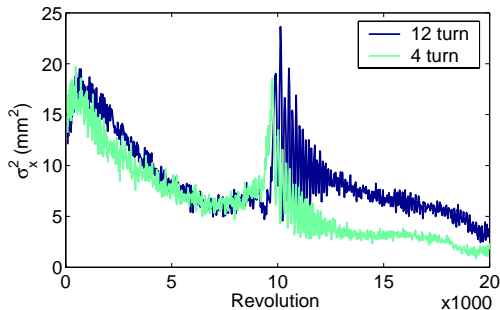


Figure 7: Horizontal beam size σ_x^2 for 4-turn and 12-turn injection. Transition crossing is at the 9600th turn.

The quadrupole mode oscillation (at twice of the synchrotron frequency) of the beam size after transition as seen in Fig. 7 was due to the phase space mismatch induced by the longitudinal space charge force, which turned from defocusing below transition to focusing above transition. We have quantitatively analyzed the behavior [1].

EMITTANCE EVOLUTION MODELING

In attempt to understand the underlying mechanism that leads to emittance growth from space charge force, we carried out 6D multi-particle tracking simulation. In the simulation the Booster is represented by a simplified model in both the longitudinal and transverse directions, but using realistic parameters recorded in the experiment. The space charge effect is modeled by assuming a Gaussian distribution.

The Booster consists of 24 combined function FODO cells. Particle transport in the transverse directions is through the 4D transfer matrix for each FODO cell. The transfer matrix was built with measured beta functions and tunes derived from turn-by-turn BPMs using the independent component analysis (ICA) method [3]. We add systematic sextupoles and small random dipole, quadrupole and skew-quadrupole errors to the model as kicks,

$$x'' + K_x x = b_0 + b_1 x + a_1 z - \frac{1}{2} b_2 (x^2 - z^2), \quad (3)$$

$$z'' + K_z z = -a_0 - b_1 z + a_1 x + b_2 x z, \quad (4)$$

where b_0 and a_0 are the dipole components, b_1 and a_1 are the quadrupole and skew-quadrupole components, respec-

tively and b_2 is the sextupole component. The random values of b_0 , a_0 , b_1 and a_1 are controlled by the amplitude

$$A_{b0}(n) = A_{b0}(0) \exp\left\{-\frac{n}{N_{dipole}}\right\} \quad (5)$$

$$A_{a0}(n) = A_{a0}(0) \exp\left\{-\frac{n}{N_{dipole}}\right\} \quad (6)$$

$$A_{b1}(n) = A_{b1}(0) \exp\left\{-\frac{n}{N_{quad}}\right\} \quad (7)$$

$$A_{a1}(n) = A_{a1}(0) \exp\left\{-\frac{n}{N_{quad}}\right\}, \quad (8)$$

where n is the turn number. The damping factor is introduced to account for decoherence. We choose $N_{dipole} = 3000$, and $N_{quad} = 4000$. The integrated sextupole strengths of the combined function magnets are -0.0173 m^{-2} and -0.263 m^{-2} for focusing and defocusing dipoles respectively for each half FODO cell. We use the rf gap voltage ramping curve recorded in experiment and assume the dipole magnets ramp linearly. The energy gain per turn are equally distributed in 18 rf cavities. The 95% longitudinal phase space area is assumed to be $0.08 \text{ eV}\cdot\text{s}$.

We assume a Gaussian charge distribution

$$\rho(x, z) = \frac{Ne}{2\pi\sigma_x\sigma_z} \exp\left\{-\frac{x^2}{2\sigma_x^2} - \frac{z^2}{2\sigma_z^2}\right\},$$

where Ne is the charge per unit length and σ_x and σ_z are the horizontal and vertical rms beam radii. Using the space charge potential found in Ref. [4], the space charge induced kick in one half-cell is then given by

$$\begin{aligned} \Delta x' &= \frac{2Nr_0\ell}{\beta^2\gamma^3\sigma_x(\sigma_x + \sigma_z)} x \exp\left\{-\frac{x^2 + z^2}{(\sigma_x + \sigma_z)^2}\right\}, \\ \Delta z' &= \frac{2Nr_0\ell}{\beta^2\gamma^3\sigma_z(\sigma_x + \sigma_z)} z \exp\left\{-\frac{x^2 + z^2}{(\sigma_x + \sigma_z)^2}\right\}, \end{aligned} \quad (9)$$

where ℓ is the length of the half cell. The space charge force is approximated by 48 localized kicks per turn. In general space charge force will change the bunch distribution so that Eq. (9) is not strictly applicable. But we still use this model since it should be valid when the deviation from the Gaussian distribution is small. This simple model allows us to test a large parameter range and investigate the physical process before it causes a significant change.

The simulation code was first checked without space charge force and sextupole components. We then introduced the space charge effects and nonlinearities and various random errors to investigate the significance of each possible mechanism.

We first examined effects of the half-integer stop band [5] by introducing quadrupole field errors with an amplitude of $40 \times 10^{-4} \text{ m}^{-1}$, or about 1.3% of the main quadrupole field. The random quadrupole errors were chosen such that the stop-band width at harmonics 12 and 13 are 0 and 0.1, respectively. We then fixed the vertical tune at $Q_z = 6.95$ and varies the horizontal tune from 6 to 7. The vertical emittance does not change in the cycle. But the

final horizontal emittance grows as the horizontal tune approaches the half-integer 6.5, as shown in Fig. 9. However, since the gradient error of the real machine is expected to be 10 times smaller, i.e., on the order of $4 \times 10^{-4} \text{ m}^{-1}$, the half-integer stopband does not explain the observed emittance growth. We also studied the Montague resonance and concluded it contributes little to emittance growth in the Booster case.

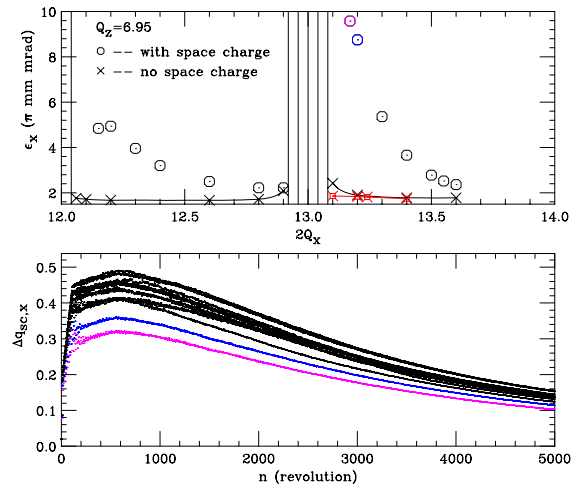


Figure 9: The final horizontal emittance (top) and space charge tune shift (bottom) for 12-turn injection.

We estimated the amplitude of the random skew-quadrupole field to be about $3.5 \times 10^{-3} \text{ m}^{-1}$, which corresponds to a vertical close-orbit error of 1 cm. We also tried several other different random skew-quadrupole levels. In the simulation we fixed the vertical tune at $Q_z = 6.85$ and varied the horizontal tune. The final emittance for a beam corresponding to 12-turn injection is plotted in Fig. 10. When the skew-quadrupole components are weak ($3.5 \times 10^{-4} \text{ m}^{-1}$), the result is almost the same as without skew-quadrupole errors. However, both the sum resonance and difference resonance become significant when the skew-quadrupole errors are $14 \times 10^{-4} \text{ m}^{-1}$ or above. The sum resonance causes large vertical emittance growth even when the resonance line is far away. We also simulated the emittance growth under different intensity level to examine the stopband width of the sum resonance. The intensity was varied from 1-turn injection to 11-turn injection. The results are shown in Fig. 11. It is seen that the stopband width increases with the beam intensity.

Dipole field errors can also cause emittance growth because the coherent kicks the beam receives from such errors can convert to emittance dilution through nonlinearities. We expect large horizontal dipole field errors since this can be generated from dipole rolls. We estimated the amplitudes of the dipole errors are about $2.0 \times 10^{-5} \text{ rad}$ for horizontal motion and $7.5 \times 10^{-5} \text{ rad}$ for vertical motion. The corresponding emittance evolution is shown in Fig. 12.

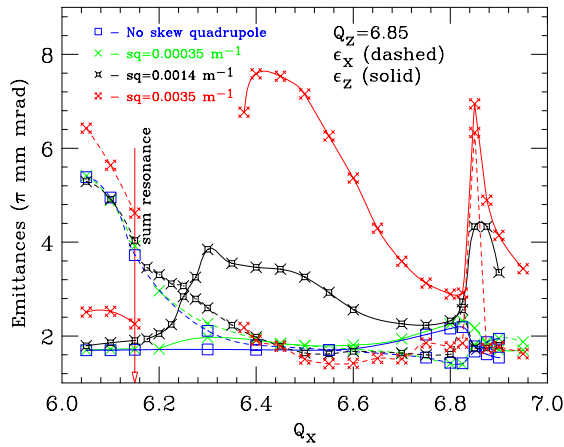


Figure 10: The final emittances for 12-turn injection beam due to space charge effect and skew-quadrupole errors.

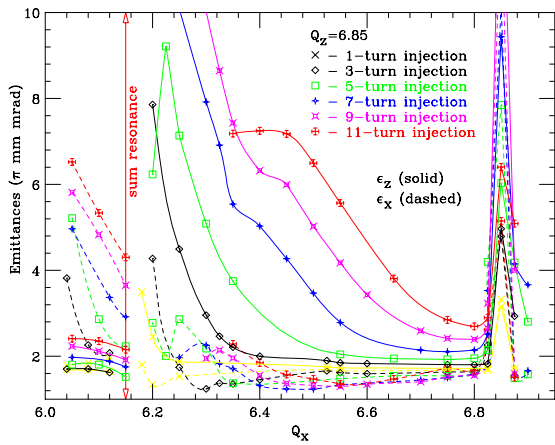


Figure 11: The final emittances for various intensity levels for random skew-quadrupole amplitude $35 \times 10^{-4} \text{ m}^{-1}$.

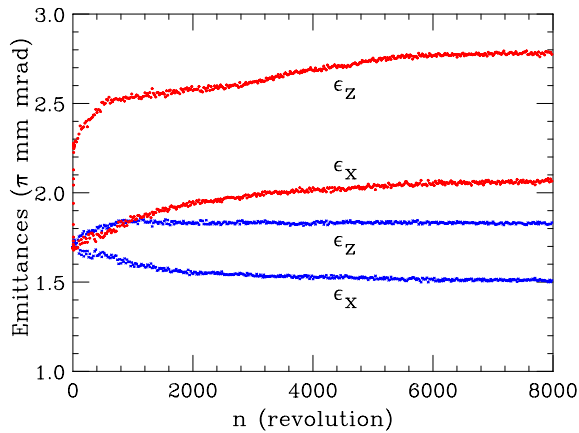


Figure 12: The emittance growth with (red) or without (blue) dipole field errors.

Finally we put all the above considered mechanisms together in the simulation. Fig. 13 shows the beam sizes at a focusing quadrupole and the emittance evolution in the cycle for a beam with 12-turn injection. In the simulation we assumed random dipole field errors (2.0×10^{-5} rad horizontal kicks 7.5×10^{-5} rad vertical kicks), random quadrupole field errors ($4.0 \times 10^{-4} \text{ m}^{-1}$) and random skew-quadrupole field errors ($35 \times 10^{-4} \text{ m}^{-1}$). The vertical emittance evolution reproduces the measurement very well in the space-charge dominated region (before 4000 turns). Emittance growth occurs mostly to the vertical plane. This is due to the combination of the random skew quadrupoles, Montague resonance and a larger dipole field error for the vertical motion. The contribution of emittance growth for the 12-turn injection is 50% due to the skew quadrupole, 25% dipole field error, and 25% from the intrinsic space-charge effects (Montague resonance). The effect of large skew quadrupole contribution is due to a large space-charge tune shift and a large linear sum resonance ($\nu_x + \nu_z = \text{integer}$).

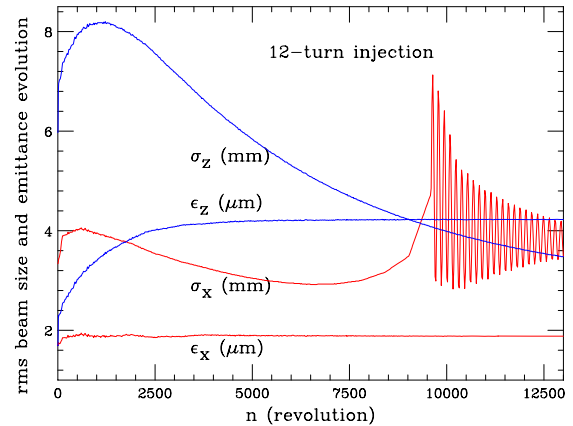


Figure 13: The rms beam sizes at a focusing quadrupole and the emittance evolution.

ACKNOWLEDGMENTS

This work was supported in part by grants from the US Department of Energy, under contract DE-AC02-76CH03000, and DE-FG0292ER40747 and the National Science Foundation NSF PHY-0552389.

REFERENCES

- [1] X. Huang et al., Phys. Rev. ST Beams 9, 014202 (2006).
- [2] J. Amundsen et al., Phys. Rev. ST Beams 6, 102801 (2003).
- [3] X. Huang et al., Phys. Rev. ST Beams 8, 064001 (2005)
- [4] S. Kheifit, PETRA Note No. 119, (1976)
- [5] F.J. Sacherer, Ph.D. Thesis, UCRL-18454 (UC Berkeley, 1968).